 CMES, vol.6, no.4, pp.349-357, 2004

Meshless Local Petrov-Galerkin (MLPG) Formulation for Analysis of Thick Plates

J. Sorić[1], Q. Li[2], T. Jarak[1] and S.N. Atluri[2]

Abstract: An efficient meshless formulation based on the Local Petrov-Galerkin approach for the analysis of shear deformable thick plates is presented. Using the kinematics of a three-dimensional continuum, the local symmetric weak form of the equilibrium equations over the cylindrical shaped local sub-domain is derived. The linear test function in the plate thickness direction is assumed. Discretization in the in-plane directions is performed by means of the moving least squares approximation. The linear interpolation over the thickness is used for the in-plane displacements, while the hierarchical quadratic interpolation is adopted for the transversal displacement in order to avoid the thickness locking effect. The numerical efficiency of the proposed meshless formulation is illustrated by the numerical examples.

keyword: meshless formulation, thick plates, three-dimensional solid concept, moving least squares approximation.

1 Introduction

During recent years, meshless approaches have attracted considerable attention due to their capability to solve a boundary value problem without a meshing procedure. In contrast to the finite element formulation, computational model is described only by a set of nodes which don't need to be connected into elements. Thus, the nodes can be easily added and removed without burdensome remeshing of the entire structure. Furthermore, by using the meshless formulation a many other difficulties associated with the finite element method may also be overcome.

In the available literature, the meshless methods for analysis of shear deformable thick plates have mostly been performed by employing Mindlin-Reissner theory [Donning and Liu (1998); Noguchi, Kawashima and Miyamura (2000); Liew, Huang and Reddy (2003); Wang and Chen (2004)]. These methods are not truly meshless because they require a background mesh for numerical integration. Furthermore, these formulations do not allow the use of general three-dimensional material law which is usual necessary for modeling of plate structural components, especially in the case of material nonlinearities. Some other formulations may be found in the literature, where a high order plate theory [Qian, Batra and Chen (2003 and 2004)] is used, but they are coupled with a large computation effort and they are time consuming. Therefore, a more efficient meshless approach for modeling of plate structures is desirable.

In this contribution, an efficient truly meshless method based on the local Petrov-Galerkin approach, originally proposed by Atluri and Zhu (1998), and later also discussed in Atluri and Shen (2002b) and Aturi (2004) is applied to the analysis of shear deformable plates with thickness to length ratio beyond 1/20. This numerical approach requires no elements or background cells in either interpolation or integration and it allows the use of complete three-dimensional constitutive laws. Using the kinematics of a three-dimensional continuum, the local symmetric weak form of the equilibrium equations over the cylindrical sub-domain, surrounding the nodes on the plate surfaces, is derived. The essential boundary conditions are enforced by a penalty method. Discretization is performed by employing the moving least squares approximation [Atluri and Shen (2002a); Li, Shen, Han and Atluri (2003)] in the in-plane directions. Analogous to the finite element formulation in Hauptmann and Schweizerhof (1998), the interpolation through the thickness is performed separately. The linear interpolation over the thickness is used for the in-plane displacements, while the hierarchical quadratic interpolation is adopted for the transversal displacement in order to avoid the undesired thickness locking effect [Sorić, Li, Jarak and Atluri (2004a and 2004b)]. The nodal unknown variables are three fictitious displacement components associated

[1] Faculty of Mechanical Engineering and Naval Architecture, University of Zagreb, Ivana Lučića 5, 10000 Zagreb, Croatia

[2] Center for Aerospace Research and Education, University of California Irvine, 5251 California Ave., Irvine, CA 92612, USA

with the nodes on the upper and lower plate surfaces. An additional unknown variable due to the hierarchical quadratic interpolation appears, and it can be eliminated by means of the static condensation. The numerical efficiency of the proposed meshless formulation is illustrated by the numerical examples.

2 Meshless formulation

According to a three-dimensional solid concept, the equilibrium equations in a domain of the volume Ω, which is bounded by the surface Γ, are given by

$$\sigma_{ij,j} + b_i = 0, \quad \text{in} \quad \Omega, \tag{1}$$

where σ_{ij} is the stress tensor and b_i denotes the body force. The indices i, j, which take the values 1, 2, 3, refer to the Cartesian coordinates x, y, z. On the boundary Γ, the following boundary conditions are assumed

$$\begin{aligned} u_i &= \overline{u}_i, \ \text{on} \ \Gamma_u, \\ t_i &= \sigma_{ij} n_j = \overline{t}_i, \ \text{on} \ \Gamma_t, \end{aligned} \tag{2}$$

where u_i are the displacement components and t_i stands for the surface traction components. Γ_u is the boundary with the prescribed displacement $\overline{u}_i$ and Γ_t is the boundary with the prescribed traction $\overline{t}_i$. n_j denotes direction cosines of the outward normal on the boundary of the volume Ω.

On applying the Meshless Local Petrov-Galerkin (MLPG) method, the equilibrium equations may be written in a weak form over the local sub-domain Ω_s

$$\int_{\Omega_s} (\sigma_{ij,j} + b_i)\, v_i \mathrm{d}\Omega - \alpha \int_{\Gamma_{su}} (u_i - \overline{u}_i) v_i \mathrm{d}\Gamma = 0. \tag{3}$$

Herein u_i is the trial function describing the displacement field, while v_i is the test function. In the MLPG method applied, the test and trial functions may be chosen from different functional spaces. The local sub-domain Ω_s is a small region inside the domain Ω and could be of any geometric shape and size. Γ_{su} is a part of the boundary $\partial\Omega_s$ of the local sub-domain with the prescribed displacement $\overline{u}_i$, and α denotes a penalty parameter, $\alpha >> 1$, which is introduced in order to satisfy the geometric boundary conditions. For plate analysis, the test function is assumed as

$$v_i = v_{oi} + z v_{i1}, \tag{4}$$

where v_{oi} and v_{1i} are arbitrary constant values. On applying the divergence theorem, after inserting (4) and some suitable rearrangement, the following local symmetric weak form is obtained

$$\begin{aligned} &\left(\int_{L_s} t_i \mathrm{d}\Gamma + \int_{\Gamma_{su}} t_i \mathrm{d}\Gamma + \int_{\Gamma_{st}} \overline{t}_i \mathrm{d}\Gamma + \int_{\Omega_s} b_i \mathrm{d}\Omega - \alpha \int_{\Gamma_{su}} (u_i - \overline{u}_i)\, \mathrm{d}\Gamma \right) v_{\mathrm{oi}} \\ &+ \left(\int_{L_s} t_i z \mathrm{d}\Gamma + \int_{\Gamma_{su}} t_i z \mathrm{d}\Gamma + \int_{\Gamma_{st}} \overline{t}_i z \mathrm{d}\Gamma + \int_{\Omega_s} (b_i z - \sigma_{i3})\, \mathrm{d}\Omega \right. \\ &\left. - \alpha \int_{\Gamma_{su}} (u_i - \overline{u}_i) z \mathrm{d}\Gamma \right) v_{1i} = 0 . \end{aligned} \tag{5}$$

As evident, the boundary $\partial\Omega_s$ of the local sub-domain is divided into three parts, $\partial\Omega_s = L_s \cup \Gamma_{st} \cup \Gamma_{su}$. L_s is the part of the local boundary inside the global domain, while Γ_{st} and Γ_{su} are the parts of the local boundary which coincide with the global traction boundary and the global geometric boundary, respectively. Since relation (5) holds for all choices of v_{oi} and v_{1i}, it yields the following expressions

$$\begin{aligned} &\int_{L_s} t_i \mathrm{d}\Gamma + \int_{\Gamma_{su}} t_i \mathrm{d}\Gamma - \alpha \int_{\Gamma_{su}} u_i \mathrm{d}\Gamma = \\ &- \int_{\Gamma_{st}} \overline{t}_i \mathrm{d}\Gamma - \int_{\Omega_s} b_i \mathrm{d}\Omega - \alpha \int_{\Gamma_{su}} \overline{u}_i \mathrm{d}\Gamma, \\ &\int_{L_s} t_i z \mathrm{d}\Gamma + \int_{\Gamma_{su}} t_i z \mathrm{d}\Gamma - \int_{\Omega_s} \sigma_{i3} \mathrm{d}\Omega - \alpha \int_{\Gamma_{su}} u_i z \mathrm{d}\Gamma = \\ &- \int_{\Gamma_{st}} \overline{t}_i z \mathrm{d}\Gamma - \int_{\Omega_s} b_i z \mathrm{d}\Omega - \alpha \int_{\Gamma_{su}} \overline{u}_i z \mathrm{d}\Gamma, \end{aligned} \tag{6}$$

which represent a set of six equations for each local sub-domain. If the local sub-domain is entirely within the global domain, all integrals over the boundaries Γ_{st} and Γ_{su} are omitted. Under the assumption of zero body force, the two domain integrations of b_i may also be eliminated.

3 Discretization and numerical implementation

The plate continuum is discretized by the nodes located on the upper and the lower surfaces, as shown in Figure 1. The nodal variables are three fictitious displacement components in the Cartesian coordinate system x, y, z. The axes x and $y$lie in the middle surface, while

z is directed over the thickness. According to the finite element formulation in Hauptmann and Schweizerhof (1998), the linear interpolation over the thickness is employed for the in-plane displacement components, while the quadratic hierarchical distribution is assumed for the transversal displacement component. Using the quadratic interpolation for the transversal displacement, the undesired so-called thickness locking effect demonstrated in Sorić, Li, Jarak and Atluri (2004a and 2004b) will be overcome. The approximation in the in-plane directions for all components is performed separately by using the Moving Least Squares (MLS) approach. Thus, the displacement distribution over the domain of influence with N couple of nodes located on the upper and the lower plate surfaces may be expressed as

$$\mathbf{u} = \sum_{J=1}^{N} \phi_J(x,y)\boldsymbol{\Psi}(z)\,\hat{\mathbf{v}}_J, \tag{7}$$

where

$$\mathbf{u}^T = \begin{bmatrix} u & v & w \end{bmatrix}, \tag{8}$$

$$\hat{\mathbf{v}}_J^T = \begin{bmatrix} \hat{u}_u & \hat{v}_u & \hat{w}_u & \hat{u}_l & \hat{v}_l & \hat{w}_l & \lambda \end{bmatrix}_J, \tag{9}$$

$$\boldsymbol{\Psi}(z) = \begin{bmatrix} \frac{1}{2}+\frac{z}{h} & 0 & 0 & \frac{1}{2}-\frac{z}{h} & & \\ 0 & \frac{1}{2}+\frac{z}{h} & 0 & 0 & \cdots & \\ 0 & 0 & \frac{1}{2}+\frac{z}{h} & 0 & & \\ & & 0 & 0 & 0 & \\ \cdots & & \frac{1}{2}-\frac{z}{h} & 0 & 0 & \\ & & 0 & \frac{1}{2}-\frac{z}{h} & \frac{1}{2}-\frac{2z^2}{h^2} & \end{bmatrix} \tag{10}$$

The in-plane components of the displacement vector $\mathbf{u}$ are represented as u and v, while w designates its transversal component. $\hat{\mathbf{v}}_J$ is the vector with the fictitious nodal displacement components on the upper and lower surfaces, denoted by indices u and l, respectively; the parameter λ is associated with the quadratic term of the transversal displacement interpolation. $\boldsymbol{\Psi}(z)$ is the interpolation matrix in the thickness direction. The value h represents the plate thickness. In relation (7), $\phi_J(x,y)$ stands for the shape function of the MLS approximation. The domain of influence mentioned above is a region where the weight functions of the nodes within it do not vanish in the local sub-domain surrounding the current nodes [Atluri and Shen (2002a)]. Equation (7) may be rewritten in the matrix form as

$$\mathbf{u} = \sum_{J=1}^{N} \boldsymbol{\Phi}_J(x,y,z)\,\hat{\mathbf{v}}_J, \tag{11}$$

where $\boldsymbol{\Phi}_J(x,y,z) = \phi_J(x,y)\boldsymbol{\Psi}(z)$. Using the derivation procedure described in Atluri and Shen (2002) and Li, Shen, Han and Atluri (2003), the shape function is obtained in the following form

$$\phi_J(\mathbf{x}) = \sum_{i=1}^{m} p_i(\mathbf{x}) \left[\mathbf{A}^{-1}(\mathbf{x})\mathbf{B}(\mathbf{x})\right]_{iJ} \tag{12}$$

with the matrices $\mathbf{A}(\mathbf{x})$ and $\mathbf{B}(\mathbf{x})$ defined as

$$\mathbf{A}(\mathbf{x}) = \sum_{J=1}^{N} W_J(\mathbf{x})\mathbf{p}(\mathbf{x}_J)\mathbf{p}^T(\mathbf{x}_J), \tag{13}$$

$$\mathbf{B}(\mathbf{x}) = \begin{bmatrix} W_1(\mathbf{x})\,\mathbf{p}(\mathbf{x}_1) & W_2(\mathbf{x})\,\mathbf{p}(\mathbf{x}_2) & \cdots \\ \ldots & W_J(\mathbf{x})\,\mathbf{p}(\mathbf{x}_J) & \ldots \quad W_N(\mathbf{x})\,\mathbf{p}(\mathbf{x}_N) \end{bmatrix}. \tag{14}$$

In the above relations $W_J(\mathbf{x})$ is the weight function associated with the node J, and $\mathbf{p}(\mathbf{x})$ denotes a complete monomial basis of order m, $\mathbf{p}^T(\mathbf{x}) = [p_1(\mathbf{x}) \;\; p_2(\mathbf{x}) \;\; \cdots \;\; \cdots \;\; p_i(\mathbf{x}) \;\; \cdots \;\; p_m(\mathbf{x})]$. $\mathbf{x}$ is the vector which contains in-plane coordinates, $\mathbf{x}^T = \begin{bmatrix} x & y \end{bmatrix}$. Here the quadratic basis and the 4^{th} order spline type weight function are assumed

$$\mathbf{p}^T(\mathbf{x}) = \begin{bmatrix} 1 & x & y & x^2 & y^2 & xy \end{bmatrix}, \tag{15}$$

$$W_J(\mathbf{x}) = \begin{cases} 1-6\left(\frac{d_J}{r_J}\right)^2+8\left(\frac{d_J}{r_J}\right)^3-3\left(\frac{d_J}{r_J}\right)^4 & 0 \le d_J \le r_J \\ 0 & d_J > r_J \end{cases} \tag{16}$$

The stress tensor components σ_{ij} may be written in a Cartesian coordinate system as 6-dimensional stress vector $\boldsymbol{\sigma}$

$$\boldsymbol{\sigma}^T = \begin{bmatrix} \sigma_x & \sigma_y & \sigma_z & \tau_{xy} & \tau_{yz} & \tau_{zx} \end{bmatrix}. \tag{17}$$

Using a generalized Hooke's law, the stress tensor components may be expressed in terms of the nodal unknown variables by the relation

$$\boldsymbol{\sigma} = \sum_{J=1}^{N} \mathbf{D}\,\mathbf{B}_J\,\mathbf{v}_J, \tag{18}$$

where **D** is the three-dimensional stress-strain matrix and $\mathbf{B}_J$ denotes the strain-displacement matrix obtained by differentiation of the shape function in a three-dimensional space

$$\mathbf{B}_J = \begin{bmatrix} (\phi_J\alpha)_{,x} & 0 & 0 & (\phi_J\beta)_{,x} & & \\ 0 & (\phi_J\alpha)_{,y} & 0 & 0 & & \\ 0 & 0 & (\phi_J\alpha)_{,z} & 0 & & \\ (\phi_J\alpha)_{,y} & (\phi_J\alpha)_{,x} & 0 & (\phi_J\beta)_{,y} & \cdots & \\ 0 & (\phi_J\alpha)_{,z} & (\phi_J\alpha)_{,y} & 0 & & \\ (\phi_J\alpha)_{,z} & 0 & (\phi_J\alpha)_{,x} & (\phi_J\beta)_{,z} & & \end{bmatrix}$$
$$\begin{bmatrix} 0 & 0 & 0 \\ (\phi_J\beta)_{,y} & 0 & 0 \\ 0 & (\phi_J\beta)_{,z} & (\phi_J\gamma)_{,z} \\ \cdots & (\phi_J\beta)_{,x} & 0 & 0 \\ (\phi_J\beta)_{,z} & (\phi_J\beta)_{,y} & (\phi_J\gamma)_{,y} \\ 0 & (\phi_J\beta)_{,x} & (\phi_J\gamma)_{,x} \end{bmatrix}, \tag{19}$$

where the following substitutions are introduced

$$\phi_J = \phi_J(x,y), \tag{20}$$

$$\alpha = \alpha(z) = \frac{1}{2} + \frac{z}{h}, \qquad \beta = \beta(z) = \frac{1}{2} - \frac{z}{h},$$
$$\gamma = \gamma(z) = \frac{1}{2} - \frac{2z^2}{h^2}, \tag{21}$$

and $(\ldots)_{,x}$ denotes the partial derivative with respect to the coordinate x.

The surface traction components t_i may also be expressed in a vector form by the relation

$$\mathbf{t} = \mathbf{N}\boldsymbol{\sigma} = \sum_{J=1}^{N} \mathbf{N}\mathbf{D}\mathbf{B}_J\mathbf{v}_J \tag{22}$$

with **N** as the matrix describing the outward normal on $\partial\Omega_s$

$$\mathbf{N} = \begin{bmatrix} n_1 & 0 & 0 & n_2 & 0 & n_3 \\ 0 & n_2 & 0 & n_1 & n_3 & 0 \\ 0 & 0 & n_3 & 0 & n_2 & n_1 \end{bmatrix}. \tag{23}$$

By means of (11), (18) and (22), equations (6) are transformed in the discretized system of linear equations which may be written in the matrix form

$$\sum_{J=1}^{N}\left[\int_{L_s}\mathbf{N}\mathbf{D}\mathbf{B}_J d\Gamma + \int_{\Gamma_{su}}\mathbf{N}\mathbf{D}\mathbf{B}_J d\Gamma - \alpha\int_{\Gamma_{su}}\boldsymbol{\Phi}_J d\Gamma\right]\mathbf{v}_J =$$
$$-\int_{\Gamma_{st}}\bar{\mathbf{t}}\,d\Gamma - \int_{\Omega_s}\mathbf{b}\,d\Omega$$
$$-\alpha\int_{\Gamma_{su}}\bar{\mathbf{u}}\,d\Gamma\sum_{J=1}^{N}\left[\int_{L_s}\mathbf{N}\mathbf{D}\mathbf{B}_J z\,d\Gamma + \int_{\Gamma_{su}}\mathbf{N}\mathbf{D}\mathbf{B}_J z\,d\Gamma\right.$$
$$\left.-\int_{\Omega_s}\mathbf{D}'\mathbf{B}'_J d\Omega - \alpha\int_{\Gamma_{su}}\boldsymbol{\Phi}_J z\,d\Gamma\right]\mathbf{v}_J =$$
$$-\int_{\Gamma_{st}}\bar{\mathbf{t}}\,z\,d\Gamma - \int_{\Omega_s}\mathbf{b}\,z\,d\Omega - \alpha\int_{\Gamma_{su}}\bar{\mathbf{u}}\,z\,d\Gamma, \tag{24}$$

where $\mathbf{D}'$ and $\mathbf{B}'_J$ are the matrices relating to the stress components σ_{i3}. The local sub-domain, where the integration is performed, is chosen as a cylinder surrounding the nodes on the upper and lower surfaces, Figure 1.

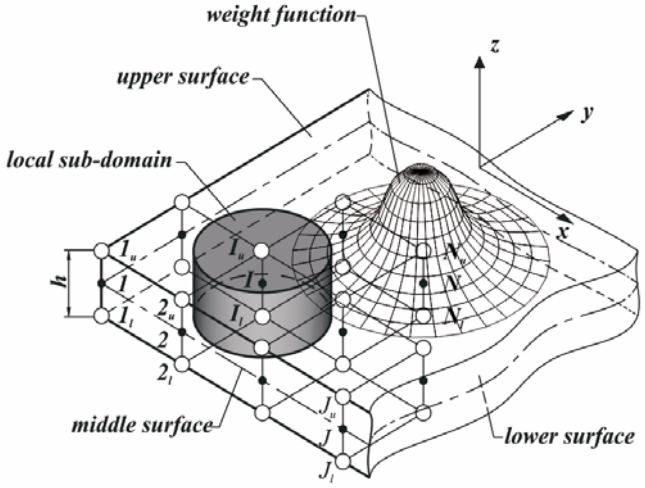

Figure 1 : Plate geometry with the local sub-domain and the weight function

If the zero body force is assumed, the two domain integrations of **b** are omitted.

As evident from (24), the six equations with seven fictitious unknowns are generated for each local sub-domain. Therefore, an additional equation is required for the solution of a boundary value problem. To obtain the addi-

tional equation, the equilibrium is enforced at the mid-point located on the middle surface within the local sub-domain Ω_s, between the nodes on the upper and the lower surfaces. The collocation method with the Dirac's Delta function $\delta(\mathbf{x}-\mathbf{x}_I)$ as the test function is employed. Accordingly, the equilibrium at the mid-point I with the position $\mathbf{x}_I = \left[\begin{array}{cc} x & y \end{array}\right]_I$ is expressed by the relation

$$\sigma_{ij,j}(\mathbf{x}_I) + b_i(\mathbf{x}_I) = 0, \tag{25}$$

which represents the three equations. Only one equation representing the equilibrium in the transversal direction is used, which is evaluated in the following discretized form under assumption of zero body force

$$\begin{array}{l} \sum_{J=1}^{N} D_0 \left[\begin{array}{ccccc} k^u_{uJ}(\mathbf{x}_I) & k^u_{vJ}(\mathbf{x}_I) & k^u_{wJ}(\mathbf{x}_I) & k^l_{uJ}(\mathbf{x}_I) \\ k^l_{vJ}(\mathbf{x}_I) & k^l_{wJ}(\mathbf{x}_I) & k^l_{\lambda J}(\mathbf{x}_I) \end{array}\right] \hat{\mathbf{v}}_J = 0, \\ I = 1,\, 2,\, \ldots,\, J,\, \ldots,\, N. \end{array} \tag{26}$$

Here the following abbreviations are introduced

$$\begin{array}{l} D_0 = \dfrac{E(1-\nu)}{(1+\nu)(1-2\nu)}, \\ k^u_{uJ}(\mathbf{x}_I) = \dfrac{\nu}{1-\nu}(\phi_J\alpha)_{,xz} + \dfrac{1-2\nu}{2(1-\nu)}(\phi_J\alpha)_{,zx}, \\ k^u_{vJ}(\mathbf{x}_I) = \dfrac{\nu}{1-\nu}(\phi_J\alpha)_{,yz} + \dfrac{1-2\nu}{2(1-\nu)}(\phi_J\alpha)_{,zy}, \\ k^u_{wJ}(\mathbf{x}_I) = \\ (\phi_J\alpha)_{,zz} + \dfrac{1-2\nu}{2(1-\nu)}(\phi_J\alpha)_{,yy} + \dfrac{1-2\nu}{2(1-\nu)}(\phi_J\alpha)_{,xx}, \\ k^l_{uJ}(\mathbf{x}_I) = \dfrac{\nu}{1-\nu}(\phi_J\beta)_{,xz} + \dfrac{1-2\nu}{2(1-\nu)}(\phi_J\beta)_{,zx}, \\ k^l_{vJ}(\mathbf{x}_I) = \dfrac{\nu}{1-\nu}(\phi_J\beta)_{,yz} + \dfrac{1-2\nu}{2(1-\nu)}(\phi_J\beta)_{,zy}, \\ k^l_{wJ}(\mathbf{x}_I) = \\ (\phi_J\beta)_{,zz} + \dfrac{1-2\nu}{2(1-\nu)}(\phi_J\beta)_{,yy} + \dfrac{1-2\nu}{2(1-\nu)}(\phi_J\beta)_{,xx}, \\ k_{\lambda J}(\mathbf{x}_I) = \\ (\phi_J\gamma)_{,zz} + \dfrac{1-2\nu}{2(1-\nu)}(\phi_J\gamma)_{,yy} + \dfrac{1-2\nu}{2(1-\nu)}(\phi_J\gamma)_{,xx}, \end{array} \tag{27}$$

In relations (27), $(\ldots)_{,xx}$ denotes the second partial derivative with respect to the coordinate x. The partial derivatives with respect to the other coordinates are denoted analogously. The values E and ν are material constants.

Now, for each local sub-domain, the system of the seven equations, expressed by (24) and (26), with seven unknowns, is derived. For the domain of influence with N couple of nodes, the set of $7N$ equations with the equal number of unknowns is evaluated. However, the parameter λ can be eliminated on the level of the domain of influence by employing a static condensation, which yields the set of equations with only fictitious nodal displacement components as unknowns.

According to the static condensation, the vector of nodal values in the domain of influence may be written as

$$\hat{\mathbf{V}}^T = \left[\begin{array}{cc} \hat{\mathbf{V}}_S & \mathbf{\Lambda} \end{array}\right], \tag{28}$$

where two subvectors $\hat{\mathbf{V}}_S$ and $\mathbf{\Lambda}$ are introduced. The subvector $\hat{\mathbf{V}}_S$ describes the nodal values on the upper and the lower plate surfaces, while $\mathbf{\Lambda}$ contains the N values of parameter λ

$$\hat{\mathbf{V}}_S^T = \left[\begin{array}{cccccc} \hat{u}_{1u} & \hat{v}_{1u} & \hat{w}_{1u} & \cdots & \hat{u}_{Nl} & \hat{v}_{Nl} \quad \hat{w}_{Nl} \end{array}\right], \tag{29}$$

$$\mathbf{\Lambda} = \left[\begin{array}{cccc} \lambda_1 & \lambda_2 & \cdots & \lambda_N \end{array}\right]. \tag{30}$$

Then, the system of equations on the domain of influence level, obtained by means of (24) and (26), may be written in the following matrix form

$$\left[\begin{array}{cc} \mathbf{K}_{VV} & \mathbf{K}_{V\Lambda} \\ \mathbf{K}_{\Lambda V} & \mathbf{K}_{\Lambda\Lambda} \end{array}\right] \left[\begin{array}{c} \hat{\mathbf{V}}_S \\ \mathbf{\Lambda} \end{array}\right] = \left[\begin{array}{c} \mathbf{F}_V \\ \mathbf{0} \end{array}\right], \tag{31}$$

where $\mathbf{K}_{VV}$, $\mathbf{K}_{V\Lambda}$, $\mathbf{K}_{\Lambda V}$, $\mathbf{K}_{\Lambda\Lambda}$ are the submatrices containing the terms associated with the unknown variables, while the vector $\mathbf{F}_V$ stands for the prescribed loading and displacement. From (31), the subvector $\mathbf{\Lambda}$ can be expressed as

$$\mathbf{\Lambda} = -\mathbf{K}_{\Lambda\Lambda}\mathbf{K}_{\Lambda V}\hat{\mathbf{V}}_S. \tag{32}$$

Finally, after substitution (32) in the first matrix equation of the system (31), the following condensed equation is obtained on the domain of influence level

$$\left(\mathbf{K}_{VV} - \mathbf{K}_{V\Lambda}\mathbf{K}_{\Lambda\Lambda}^{-1}\mathbf{K}_{\Lambda V}\right)\hat{\mathbf{V}}_S = \mathbf{F}_V. \tag{33}$$

On the structural level, the global set of equations is derived by using the well-known numerical procedure.

4 Numerical examples

4.1 Clamped square plate

A clamped square plate subjected to the uniformly distributed load over the upper surface is considered first. The plate thickness to span ratio is $h/a = 0.1$. The material data are Young's modulus $E = 10.92 \cdot 10^5$ and Poisson's ratio $\nu = 0.3$. Due to symmetry, only one quarter of the plate is discretized by the various uniformly distributed grid points on the upper and lower plate surfaces. The discretization by 9x9 nodes is shown in Figure 2.

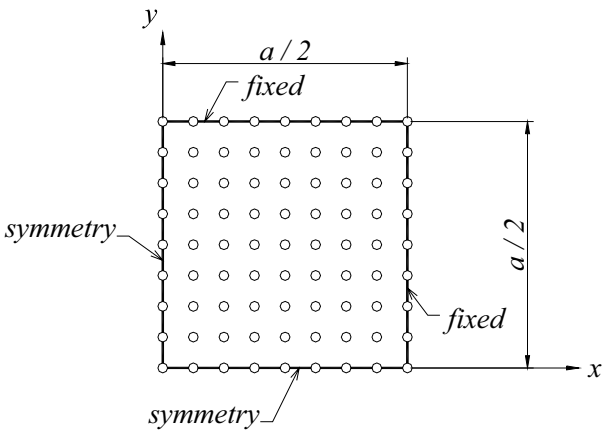

Figure 2 : Discretization of one quarter of the square plate surface

The influence of the radius of the weight function circular support on the plate central deflection is investigated. It is found that the weight function support significantly affects the numerical solutions. Dependency of the plate central deflection on the ratio of the support radius to the radius of local sub-domain for different number of grid points is plotted in Figure 3.

The deflection is normalized by using the exact analytic solution from Srinivas and Rao (1973). As evident, the noticeable oscillations around the exact value are exhibited. The convergence to the exact solution with the increase of the grid size is achieved for the ratio of the support radius to the radius of local sub-domain of 2.9. The convergence rate of the central deflection is plotted in Figure 4.

In this figure, the results are compared with the values obtained by the algorithm derived in Sorić, Li, Jarak and Atluri (2004a), where the linear distribution of the

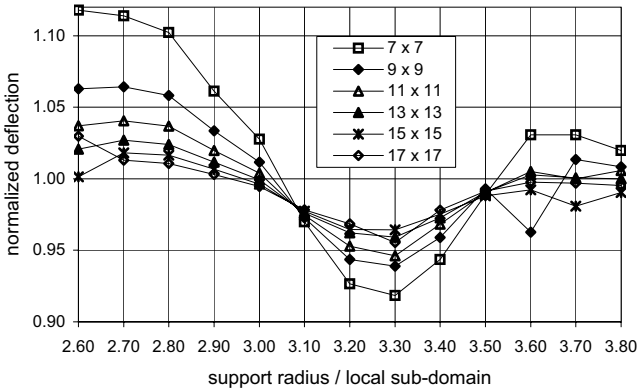

Figure 3 : Central deflection of the clamped plate

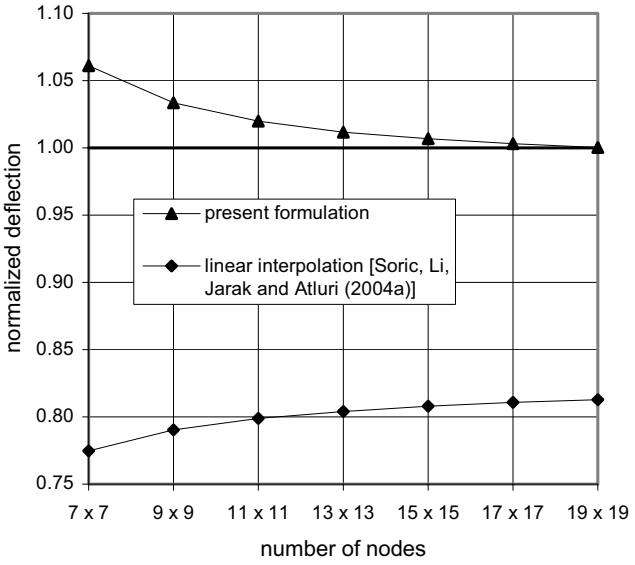

Figure 4 : Convergence of the central deflection of the clamped plate

transversal displacement in the plate thickness direction is assumed. As may be seen, the curve representing the linear interpolation shows the significant locking effect [Hauptmann and Schweizerhof (1998)] which is eliminated by using the present formulation. The results of the convergence study are also compared with the finite element solutions obtained by linear 3D brick-type elements by using the program package NASTRAN, as shown in Figure 5.

The figure represents the normalized transversal displacement on the center of the middle plate surface versus the number of degrees of freedom plotted on a log-

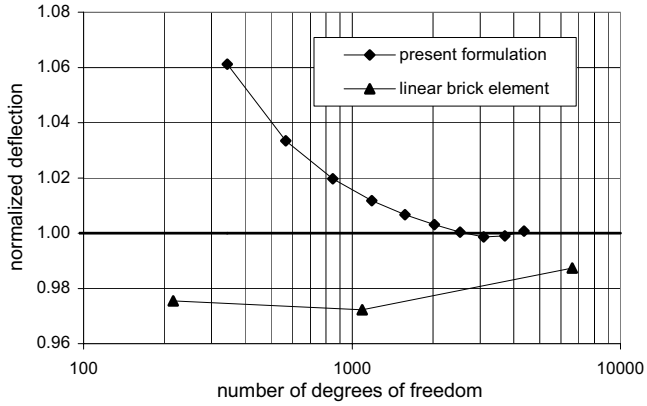

Figure 5 : Convergence study in comparison with the finite element solutions for the clamped plate

arithmic scale. As obvious, in contrast to the meshless results which converge to the analytical solution, the convergence of the finite element solutions is not exhibited. Like the MLPG formulation from Sorić, Li, Jarak and Atluri (2004a), the linear brick elements show a tendency to lock because of coupling between the normal stress in the thickness direction and the strains in the in-plane directions. To improve the finite element results, more elements in the thickness direction are necessary [Hauptmann and Schweizerhof (1998)]. The deformed plate configuration discretized by the grid of the 17x17 nodes on each plate surfaces is plotted in Figure 6.

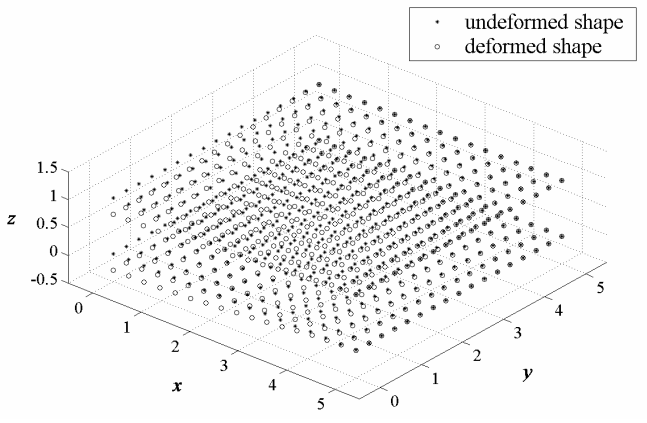

Figure 6 : Deformed plate configuration

4.2 Simply supported square plate

As the second example, the simply supported square plate under uniformly distributed load over the upper surface is analyzed. The geometry and material data are the same as in the first example. Here only the boundary conditions are replaced. Instead of the fixed boundary of the clamped plate, only the transversal displacements are suppressed along the simply supported boundary. Like in the first example, the convergence rate is presented in Figure 7, where the normalized central deflection is compared with the finite element solutions obtained by NASTRAN.

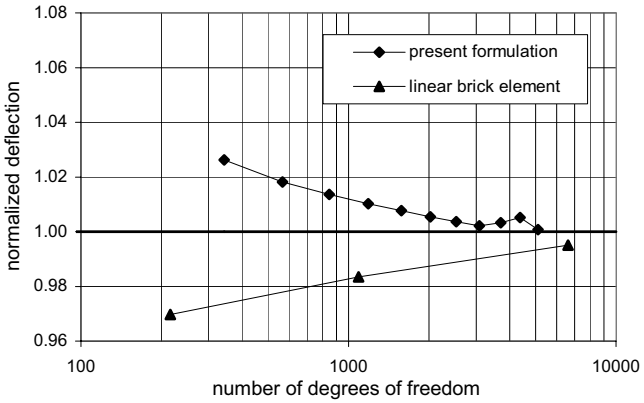

Figure 7 : Convergence study in comparison with the finite element solutions for the simply supported plate

The analytical value used for the normalization is also taken from Srinivas and Rao (1973). As in the case of the clamped plate, the results obtained by the linear brick elements do not achieve the exact solution. The normalized displacements computed by the present formulation in comparison with those obtained by the formulation presented in Sorić, Li, Jarak and Atluri (2004) are plotted in Figure 8. The differences between the curves associated with the present formulation and the formulation from Sorić, Li, Jarak and Atluri (2004) are also exhibited.

5 Conclusion

An efficient meshless formulation based on the Local Petrov-Galerkin approach has been applied to the analysis of thick plates. This numerical method is truly meshless because no elements or background cells are involved in either interpolation or integration. Using the

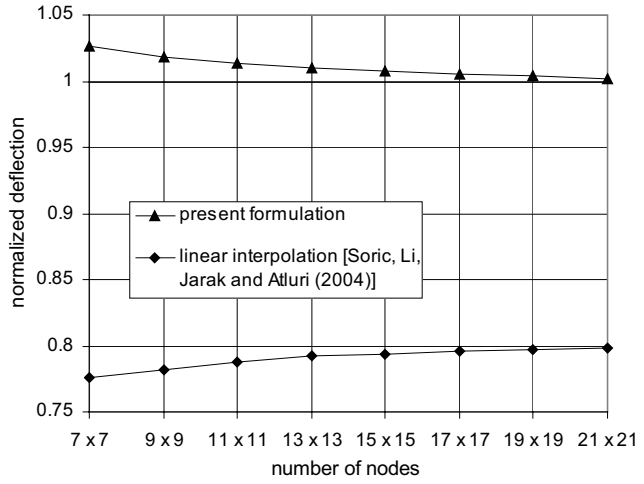

Figure 8 : Convergence of the central deflection of the simply supported plate

kinematics of a three-dimensional continuum, the local symmetric weak form of the equilibrium equations over the cylindrical local sub-domain is derived. The linear test function over the plate thickness is adopted, and the essential boundary conditions are enforced by applying the penalty method. The moving least squares approximation is employed for discretization in the in-plane directions. In contrast to the linear interpolation over the thickness for the in-plane displacement components, the hierarchical quadratic approximation is applied for the transversal displacement, which yields the elimination of the thickness locking effect. The nodal unknown variables are three fictitious displacement components associated with the nodes on the upper and lower plate surfaces. An additional unknown variable due to the hierarchical quadratic interpolation is eliminated by using the static condensation on the domain of influence level. By properly choosing the radius of the circular support of the weight function, a good convergence rate of the numerical results is exhibited as shown by numerical examples.

Acknowledgement: The first author expresses his gratitude to the Fulbright Foundation for the granted financial support by Fulbright scholarship.

References

Atluri, S. N.; Zhu, T. (1998): A new Meshless Local Petrov-Galerkin (MLPG) approach in computational mechanics. *Comput. Mech.* 22, 117-127.

Atluri, S. N.; Shen, S. (2002a): *The Meshless Local Petrov-Galerkin (MLPG) Method*, Tech. Science Press, Encino, USA.

Atluri, S. N.; Shen, S. (2002b): The Meshless Local Petrov-Galerkin (MLPG) Method: A Simple & Less-costly Alternative to the Finite Element and Boundary Element Methods, *CMES: Computer Modeling in Engineering & Sciences* 3 (2002), 11-51.

Atluri, S. N. (2004): *The Meshless Method (MLPG) for Domain and BIE Discretizations*, Tech Science Press, 2004, 688 pages

Donning, B. M.; Liu, W. K. (1998): Meshless methods for shear-deformable beams and plates. *Comput. Methods Appl. Mech. Engrg.* 152, 47-71.

Hauptmann, R.; Schweizerhof, K. (1998): A systematic development of solid-shell element formulations for linear and non-linear analyses employing only displacement degrees of freedom, *Int. J. Numer. Meth. Engng*, 42, 49-69.

Li, Q.; Shen, S.; Han, Z. D; Atluri, S. N. (2003): Application of Meshless Local Petrov-Galerkin (MLPG) to Problems with Singularities, and Material Discontinuities, in 3-D Elasticity, *CMES: Computer Modeling in Engineering & Sciences* 4, 571-585.

Liew, K. M.; Huang, Y. Q.; Reddy, J. N. (2003): Moving least squares differential quadrature method and its application to the analysis of shear deformable plates, *Int. J. Numer. Meth. Engng.* 56, 2331-2351.

Long, S.; Atluri, S. N. (2002): A Meshless Local Petrov-Galerkin Method for Solving the Bending Problem of a Thin Plate, *CMES: Computer Modeling in Engineering & Sciences* 3, 53-63.

Noguchi, H.; Kawashima, T.; Miyamura, T. (2000): Element free analyses of shell and spatial structures, *Int. J. Numer. Meth. Engng.* 47, 1215-1240.

Qian, L. F.; Batra, R. C.; Chen, L. M. (2003): Elastoplastic Deformations of a Thick Plate by using a Higher-Order Shear and Normal Deformable Plate Theory and two Meshless Local Petrov-Galerkin (MLPG) Methods, *CMES: Computer Modeling in Engineering & Sciences* 4, 161-175.

Qian, L. F.; Batra, R. C.; Chen, L. M. (2004): Static and dynamic deformations of thick functionally graded elastic plates by using higher-order shear and nor-

mal deformable plate theory and meshless local Petrov-Galerkin method, *Composites*, in press.

Sorić, J.; Li, Q.; Jarak, T.; Atluri, S. N. (2004a): On the application of the meshless Local Petrov-Galerkin (MLPG) Method to the Analysis of Shear Deformable Plates, Proceedings of the 2004 International Conference on Computational & Experimental Engineering and Sciences, Tadeu, A.; Atluri S.N. (eds.), CD-ROM-Edition, Madeira, Portugal.

Sorić, J.; Li, Q.; Jarak, T.; Atluri, S. N. (2004b): An Efficient Meshless Formulation for Thick Plate Analysis, Proceedings of the WCCM VI: Sixth World Congress on Computational Mechanics, Yao, Z.H.; Yuan, M.W.; Zhong, W.X. (eds), CD-ROM-Edition, Beijing, China.

Srinivas, S.; Rao, A. K. (1973): Flexure of Thick Rectangular Plates, *J. Appl. Mech. ASME*, 40, 298-299.

Wang, D.; Chen, J.-S. (2004): Locking-free stabilized conforming nodal integration for meshfree Mindlin-Reissner plate formulation, *Comput. Methods. Appl. Mech. Engrg.* 193, 1065-1083.